# DGS-Integrated Air-Loaded Wideband Microstrip Antenna for *X*- and *Ku*-Band

Tanmoy Sarkar, *Student Member, IEEE*, A. Ghosh, L. L. K. Singh, Sudipta Chattopadhyay, *Member, IEEE*, and Chow-Yen-Desmond Sim, *Senior Member, IEEE*

***Abstract*—Over the past few years, there has been a huge demand to design a simple printed antenna for high-speed multimedia communication with low cost, compact size, wide band, and low copolarization (CP) to cross-polarization (XP) isolation levels. In this letter, a simple and completely planar air-gap-loaded rectangular microstrip antenna integrated with single shorting post and defected ground structures has been thoroughly investigated to obtain wide bandwidth of 58.72% (8.3–15.2 GHz) at *X*- and *Ku*-band. Besides exhibiting good broadside patterns and desirable gain (>5 dBi), good CP-to-XP isolation levels (16 dB) are also achieved. Furthermore, the proposed antenna has a low profile of 0.083 $\lambda_0$.**

***Index Terms*—Air-gap loading, rectangular microstrip antenna (RMA), wideband antenna.**

## I. Introduction

WIDEBAND printed antennas are very much exigent due to the advantages such as invulnerability to jamming, fading in multipath environment, and low power consumption that increases battery life. For military applications such as high-resolution RF imaging radar and jamming technology for military airborne systems, their operating bands are usually at *X*- and *Ku*-band. Thus, wideband antenna designs that can cover these bands are now the topics of interest.

The rectangular microstrip antenna (RMA) is a very much simple genre of tiny printed antennas that usually suffers from narrow impedance bandwidth (3% to 5%) and undesirable copolarization-to-cross-polarization (CP–XP) isolation (usually 8–10 dB) across the *X*-band [1]. Amid all the design methods, one simple way to improve the bandwidth is to apply the stacked patch [2]. To further enhance the bandwidth and efficiency, the use of air-gap-loaded RMA has recently attracted a lot of attention to yielding a simple printed antenna with wide bandwidth. In fact, the widespread use of finite air gap in different antenna configurations has been investigated intensively over the last two decades [3]–[7], for widening the bandwidth of RMA. In recent years, mode merging techniques have been employed to achieve wide impedance bandwidth from low-frequency MAs [10]–[12] of 18%–27% impedance bandwidth. However, in all the cases, the E-plane radiation pattern contains null radiation at its broadside (conical radiation pattern), whereas the H-plane radiation pattern shows bore-sight radiation that is not enviable from a true broadside antenna. In [13], a wideband RMA with two parasitic mushroom-type arrays loaded along the two radiating edges of RMA has been reported employing dominant $TM_{10}$ and higher order quasi-$TM_{30}$ modes to exhibit 40% impedance bandwidth at *Ku*-band. Nevertheless, the MAs reported in [2]–[13] are complex to design and difficult to fabricate as well. Recently, a number of techniques have also been applied on MA design to satisfy the *Ku*- or *X*/*Ku*-band. In [14], a slotted planar patch antenna (size of $20 \times 14 \times 1.6$ mm$^3$) with 7.7% (1380∼1853 MHz) impedance bandwidth is reported. To double the bandwidth to 15.5% (1310∼1530 MHz) for a slot antenna, the work in [15] used a single-layer metamaterial superstrate. Even though this design has achieved a high peak gain of 13.78 dBi, it has a volume size of $60 \times 60 \times 14$ mm$^3$. To improve the operating bandwidth with compact size, Lakrit *et al.* [16] presented an edge-fed RMA with 22.7% (1080–1355 MHz) bandwidth that has an overall size of $18 \times 20 \times 1.58$ mm$^3$. However, the radiation patterns exhibited in this work are highly unstable over the bands of interest. As for the work reported in [17], by applying the stacked method (three layers, dielectric-air-dielectric) with defected ground structure (DGS), very wide bandwidth of 52.72% (11.97–20.54 GHz) that can cover the desired *Ku*/*K*-band has been achieved, and the overall size of this MA antenna is $20 \times 20 \times 4.8$ mm$^3$. Nevertheless, there is no further evidence nor discussion that stable radiation patterns can be achieved across the bands of interest. Notably, the above reported works [14]–[17] have exhibited very high gain variation across the bands of interest, which is not desirable and will be further discussed. The incorporation of DGS in MA is an established technique to enhance its performance. Although it is widely used to improve polarization purity of RMA [18], there are very few reports available [19]–[22] where the technique is utilized to overcome the narrow bandwidth issue of RMA. In those reports, maximum 22% bandwidth has been obtained from simple DGS integrated RMA. By observing the above works, it is realized that DGS integrated air-gap-loaded probe-fed RMA is not investigated earlier for achieving wide impedance bandwidth in the *X*- and *Ku*-band. Therefore, in this letter, a DGS integrated air-gap-loaded RMA with a shorting post is studied. Besides achieving wide impedance bandwidth of 58.72% (8.38–15.2 GHz) across the *X*- and *Ku*-band, the proposed RMA can still maintain desirable CP–XP isolation level and stable gain variation. Furthermore, the proposed structure is very simple, and it is easy to manufacture as well.

Manuscript received October 23, 2019; accepted November 16, 2019. Date of publication November 22, 2019; date of current version January 20, 2020. *(Corresponding author: Sudipta Chattopadhyay.)*

T. Sarkar is with the Mizoram University, Aizawl 796004, India, and also with the Burdwan University, Bardhaman 713 104, India (e-mail: 2005.tanmoy@gmail.com).

A. Ghosh, L. L. K. Singh, and S. Chattopadhyay are with the Mizoram University, Aizawl 796004, India (e-mail: abhijyoti_engineer@yahoo.co.in; llksingh@yahoo.co.in; sudipta_tutun@yahoo.co.in).

C.-Y.-D. Sim is with the Department of Electrical Engineering, Feng Chia University, Taichung 40724, Taiwan (e-mail: cysim@fcu.edu.tw).

Digital Object Identifier 10.1109/LAWP.2019.2955111

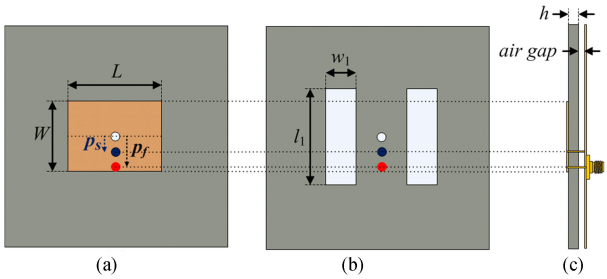


Fig. 1. Detailed dimensions of the proposed antenna structure. (a) Front. (b) Back. (c) Side plane. White dot represents the center position of the patch, blue dot represents the shorting post (or via), and red dot represents the feeding position. $L = 8.0$, $W = 12$, $p_s = 2.0$, $p_f = 3.4$, $l_1 = 16$, $w_1 = 10$, *air gap* $= 1.0$, $h = 1.575$. Unit: mm. The rectangular patch and square ground sizes are not drawn to scale.

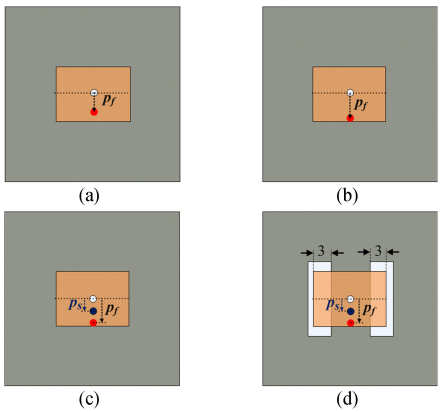


Fig. 2. Design evolution of the proposed antenna structure. White dot represents the center position of the patch, blue dot represents the shorting post (or via) position $p_s$ with reference to center position, and red dot represents the feeding position $p_f$ with reference to the center position. (a) Antenna#1, conventional RMA without air gap and $p_f = 2.6$. (b) Antenna#2, conventional RMA with air gap and $p_f = 3.8$. (c) Antenna#3, Proposed without DGS, $p_s = 2.0$ and $p_f = 3.8$. (d) Antenna#4 (Proposed), $p_s = 2.0$ and $p_f = 3.4$. Unit: mm.

## II. Antenna Design Structure

The radiating patch dimension of 8 mm ($L$) $\times$ 12 mm ($W$) is printed on RT duroid substrate ($\varepsilon_r = 2.33$, thickness $h =$ 1.575 mm) of size 60 mm $\times$ 60 mm as shown in Fig. 1. Following [23], the *W/L* ratio is considered to be 1.5. The ground plane is made of 0.5 mm thick copper plate. An air gap of thickness 1 mm gap has been introduced between the ground plane and the substrate. The shorting post (or via) of radius of 0.6 mm is positioned at $p_s = 2$ mm with reference to the center position (white dot) of the patch. The probe feed of radius of 0.6 mm is located at 3.4 mm $(p_f)$ from the center position of the patch. Finally, two DGSs (each of size 16 mm $\times$ 10 mm) are loaded into the copper ground plane, and the defects penetrate laterally 3 mm beneath the patch from both sides, as shown in Fig. 2(d).

## III. Evolution Analysis of Proposed Antenna

To comprehend the final design of this proposed antenna, its design evolution is shown in Fig. 2. All simulation and optimization is conducted by the commercial electromagnetic software HFSS [24]. First, a conventional RMA with patch dimension 8 mm $\times$ 12 mm is designed on a grounded RT duroid substrate with thickness 1.575 mm for *X*-band (10.9 GHz). The

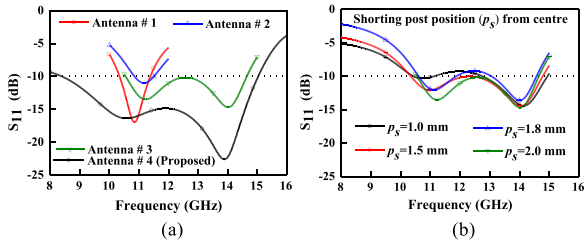


Fig. 3. (a) Reflection coefficient profiles for Antenna#1, Antenna#2, Antenna#3, and Antenna#4 (proposed antenna). (b) Reflection coefficient profiles for Antenn#3 when tuning $p_s$ from 1.0 to 2.0 mm.

corresponding optimized feed position is $p_f = 2.6$ mm, and it is known as reference antenna (Antenna#1), as shown in Fig. 2(a). Fig. 3(a) shows the simulated reflection coefficients of Antenna#1, which exhibits a resonance at 10.9 GHz with good impedance matching. Next, 1 mm air gap has been introduced between substrate and ground plane of Antenna#1, and the new optimized feed position is $p_f = 3.8$ mm. It is denoted as Antenna#2, as shown in Fig. 2(b). As depicted in Fig. 3(a), the resonant frequency is increased to 11.2 GHz, and the matching of the Antenna#2 is poorer than Antenna#1. As shown in Fig. 2(c), in order to achieve wider operating bandwidth, we have realized that loading a shorting post at position $p_s = 2$ mm can excite an additional resonance mode in the higher frequency band, forming dual resonances that can cover wide impedance bandwidth of 32.47% (10.55–14.64 GHz) as shown in Fig. 3(b) for Antenna#3. Here, it is further observed that as the position of the shorting post $(p_s)$ is moving away the feeding probe position towards the center (from $p_s = 2$ mm to $p_s = 1$ mm), the frequency ratio of the dual resonances will become larger and the two resonances will eventually break away from each other, showing two separated resonances.

In the final design step, a pair of slot DGS with dimensions 16 mm $\times$ 10 mm are loaded into the copper ground, near the two nonradiating edges of the patch. In this case, $p_s$ and $p_f$ are set to be 2 mm and 3.4 mm, respectively, and it is now Antenna#4 (or proposed antenna), as shown in Fig. 2(d). Here, the main reason for doing so is to further widen the impedance bandwidth and at the same time improving the CP–XP isolation. The effects of the slot DGS dimension on the final antenna structure are not shown in this letter, for brevity. By further optimizing the proposed antenna, from Fig. 3(a) it can be observed that Antenna#4 can achieve very wide 10 dB impedance bandwidth of 56.7% (8.39–15.03 GHz) (simulated).

The H-plane radiation characteristics of Antenna#2, Antenna#3, and Antenna#4 (proposed) are plotted in Fig. 4 at 10.6 GHz. As can be seen, there is no significant change in the CP radiation profile for all three cases. However, one can see that Antenna#2 has high XP radiation, and in this case, the CP–XP isolation is around 5 dB (see upper hemisphere especially within $\pm 60^\circ$). This XP radiation level becomes even worse for Antenna#3, and in this case, the XP level is higher than the CP level by 5 dB. Therefore, it also fails to improve the polarization purity. On the contrary, after loading the DGS, the minimum CP–XP isolation is around 16.5 dB, and within $-30^\circ$ to $+30^\circ$, this CP–XP isolation is improved to more than 20 dB. Hence, XP radiation level is significantly reduced in the case of the Antenna#4. As there are no significant changes in the E-plane radiation pattern, the results are omitted here for brevity.

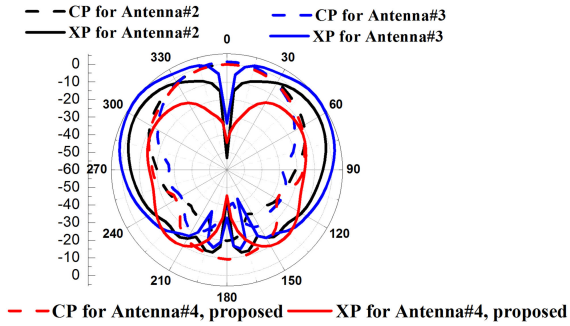


Fig. 4. Normalized H-plane ($yz$ plane) radiation patterns of Antenna#2, Antenna#3 and Antenna#4 (proposed) at 10.6 GHz.

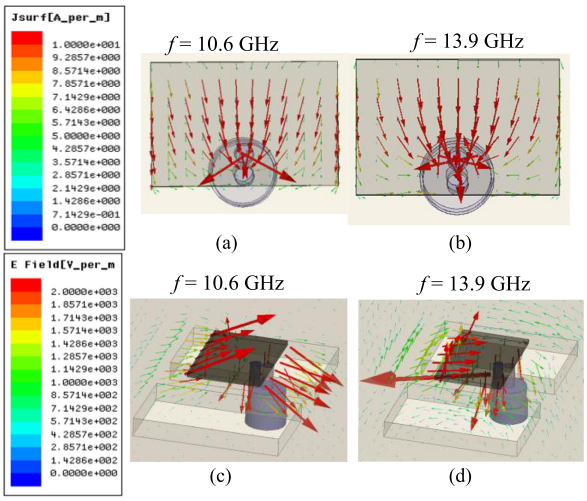


Fig. 5. Electric surface current distribution on the rectangular patch surface at (a) $f = 10.6$ GHz and (b) $f = 13.9$ GHz. Electric field vectors within the substrate at (c) $f = 10.6$ GHz and (d) $f = 13.9$ GHz.

## IV. Bandwidth Enhancement Technique

The narrow bandwidth of the conventional RMA is improved by introducing an air gap between the substrate and ground plane, which in turn lowers the effective permittivity of the substrate and consequently enhances the bandwidth of the RMA as bandwidth $\propto 1/\sqrt{\varepsilon_r}$. Even though the impedance matching for such a case is poor, it can still achieve approximately 8% impedance bandwidth. In general, the optimum feed location shifts towards the edge of the patch in air-gap-loaded structure [25]. Therefore, the impedance of the patch near the edge is very high, and hence it causes problem in impedance matching. Now, in order to achieve two fold advantages in terms of matching and bandwidth, a shorting post is placed near the feeding probe. Accordingly, the impedance near the feed probe is reduced due to the enhancement of magnetic fields at the vicinity of the shorting post (near the probe), which improves the impedance matching and hence offers better impedance bandwidth than the earlier one. Furthermore, the shorting post beneath the patch introduces an additional resonance, which is occurring at 13.9 GHz along with the fundamental resonance at 10.6 GHz.

The simulated electric surface currents (on the patch) and electric field vectors (within the substrate) at these two resonances ($f = 10.6$ GHz and $f = 13.9$ GHz) of the proposed structure (Antenna#4) are depicted in Fig. 5. Here, the profiles of the electric surface currents at both the frequencies in Fig. 5(a) and (b) are similar to $TM_{10}$ mode, and they will produce broadside

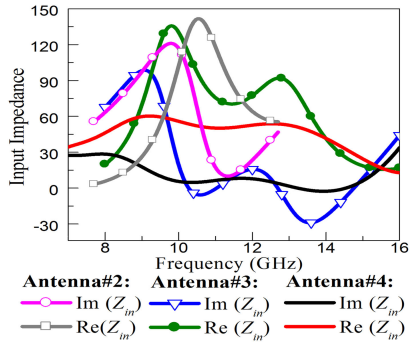


Fig. 6. Input impedances of Antenna #2, Antenna #3, and Antenna #4.

radiations with similar polarizations. By further observing the electric field vectors in Fig. 5(c), it reveals that the radiations are taking place from both the upper and lower radiating edges at $f = 10.6$ GHz. In contrast, Fig. 5(d) shows that at $f = 13.9$ GHz, the radiation takes place mainly from the upper radiating edge. Close inspection of the structure at these two frequencies further reveals that the first mode ($f = 10.6$ GHz) resonates between the two radiating edges (upper and lower), and thus the structure is working as a half-wave patch ($L_1 = \lambda/2$). As for the second mode ($f = 13.9$ GHz), the same structure resonates between the upper radiating edge of the patch and the shorting post, and hence it acts as $3\lambda/8$ patch ($L_2 = 3\lambda/8$). Therefore, the frequency ratio of the two excited frequencies is small (i.e., $f_2/f_1 = L_1/L_2 = 1.33$), and they eventually merge into each other and offer broader bandwidth. Notably, the presence of slot DGS at the ground plane further extends the lower limit of the operating band by altering the return current path. In fact, as the current travel across the discontinuity between ground plane and slot defect, a portion of the current switches into displacement current and it induces a capacitance $C$, whereas the other part of the current is redirected at the vicinity of the corners of the slot, which causes the current to travel an extra path and induces an inductance $L$. The effect of these two factors incorporates a net phase shift in the return path of current, and as a result, it slows down the current flow. Hence, the lower frequency limit (operating band) of the antenna shifts towards the lower side of the spectrum.

The input impedance profiles of Antenna#2, Antenna#3, and Antenna#4 are depicted in Fig. 6. Here, the evidence of dual resonances in close proximity is clearly revealed for Antenna#3 in comparison with Antenna#2. Furthermore, as compared with the other two, the proposed antenna structure (Antenna#4) has exhibited lower variation of input impedance (real and imaginary), which is also one of the reasons for achieving wider bandwidth.

## V. Results and Discussions

The measurements have been conducted with proposed fabricated antenna as shown in Fig. 7. As depicted in Fig. 8(a), the measured 10 dB impedance bandwidth of the proposed antenna was 58.72% (8.3–15.2 GHz). Compared with the simulated one (56.7%, 8.39–15.03 GHz), even though the two resonances have shown different $S_{11}$ values (maybe due to fabrication tolerances), the overall performances between the measured and simulated reflection coefficients are almost the same. As aforementioned, one of the main features of this letter is the stability of gain. By observing Fig. 8(b), one can see that the measured gain variation of the proposed antenna was

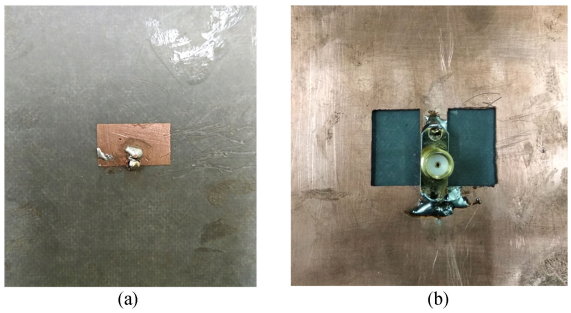

(a) (b)

Fig. 7. Photographs of proposed antenna (partial view). (a) Front. (b) Back.

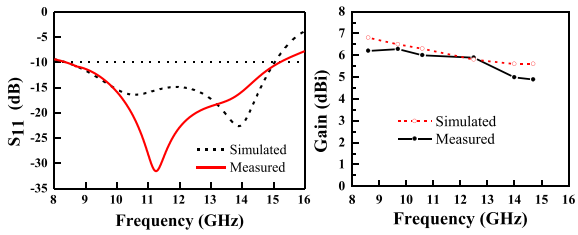


(a) (b)

Fig. 8. Measured and simulated results of the proposed antenna. (a) Reflection coefficient profile. (b) Gain variation profile.

between 5 and 6.5 dBi across the bands of interest, which is in good agreement with simulation results (5.6–6.8 dBi). Here, it is also noteworthy to mention that the measured radiation efficiencies were 71%–94%. Fig. 9(a)–(c) shows the measured and simulated radiation patterns (H- and E-plane) at 9.7, 12.5, and 14.7 GHz, respectively. Furthermore, the H-plane radiation patterns in all the frequencies are excellently stable with no distortion across the entire operating band, and desirable CP–XP isolation of approximately 16 dB is also achieved. By further observing Fig. 9, the E-plane radiation patterns of the proposed antenna reveal a good broadside radiation in the entire operating band. Notably, a reduced radiation (null) in the E-plane at off-bore-sight direction is observed at higher frequencies (12.5 and 14.7 GHz), and it is due to leakage radiation from the probe through the ground plane defect. It may be noted that the proposed antenna has poor front-to-back (*F/B*) radiation isolation, which is common for wideband patches [26]–[29]. In fact, the field bouncing effect due to shorting post along with the leakage of radiation through slot DGS is responsible for such low *F/B* radiation isolation, especially at higher frequencies. This can be improved using the method described in [30]. The beam efficiency of the proposed antenna is around 65%, which causes $G/T = -13$ dB/K. Following [31], $G/T = -15$ dB/K is suitable for mobile communication environment and handheld devices, and hence the proposed antenna structure can be useful for communications between handheld devices and also in other military wireless applications.

Further measurement has also shown stable 3 dB beamwidth of 70°−65° and 110°−90° in the H- and E-plane, respectively, across the whole band (8.3–15.2 GHz), but it is not shown for brevity. Thus, the proposed antenna has demonstrated very stable patterns (and gain variation as well). Table I shows the performances of the proposed antenna in comparison with the references [13]–[17]. Here, even though the proposed antenna may have exhibited slightly larger planar size, it can still maintain a low profile of $0.083\lambda_0$. Besides that, it has shown

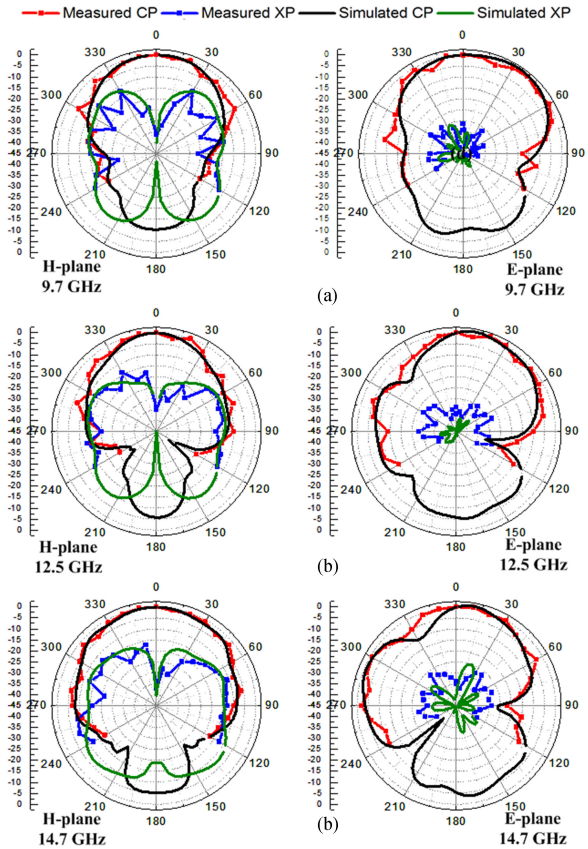


Fig. 9. Simulated and measured radiation patterns at H-plane (*yz* plane) and E-plane (*xz* plane) across different frequencies. (a) $f = 9.7$ GHz. (b) $f = 12.5$ GHz. (c) $f = 14.7$ GHz.

TABLE I
PERFORMANCES COMPARISON OF PROPOSED ANTENNA WITH REFERENCES

| Ref | Size ($mm^3$) ($\lambda_0$ @ lowest freq.) | BW (%) Freq. Range (GHz) | CP-XP Isolation (dB) | Gain Variation (dBi) |
|---|---|---|---|---|
| [13] | 20×32×1.5<br>$0.79\lambda_0\times1.4\lambda_0\times0.065\lambda_0$ | 41.86%<br>11.90–18.20 | 11 | 10–10.5 |
| [14] | 20×14×1.6<br>$0.92\lambda_0\times0.61\lambda_0\times0.07\lambda_0$ | 7.73%<br>13.80–18.53 | 13 | –2.5–7.8 |
| [15] | 60×60×14<br>$2.62\lambda_0\times2.62\lambda_0\times0.611\lambda_0$ | 15.5%<br>13.10–15.30 | NA | 7.2–13.78 |
| [16] | 18×20×1.58<br>$0.65\lambda_0\times0.72\lambda_0\times0.057\lambda_0$ | 22.59%<br>10.80–13.55 | NA | 1.3–4.91 |
| [17] | 20×20×4.8<br>$0.8\lambda_0\times0.8\lambda_0\times0.192\lambda_0$ | 52.72%<br>11.97–20.54 | NA | –6–8.5 |
| **PA** | **60×60×3**<br>$\mathbf{1.66\lambda_0\times1.66\lambda_0\times0.083\lambda_0}$ | **58.72%**<br>**8.30–15.20** | **16.5** | **5–6.5** |

BW∼bandwidth, PA∼proposed antenna, NA∼not applicable.

very wide bandwidth of >58% and good CP–XP isolation of 16.5 dB. Finally, it has also exhibited very stable radiation patterns across the bands of interest with stable gain variation of no more than 1.5 dB.

## VI. CONCLUSION

A simple planar single-element RMA has been successfully investigated for wideband applications in *X*- and *Ku*-bands. Besides achieving wide bandwidth of 58.72%, the proposed antenna has also demonstrated stable radiation pattern, gain variation, and desirable CP–XP level across the entire band of interest.

## REFERENCES


[1] R. Garg, P. Bhatia, I. Bahl, and A. Ittipiboon, *Microstrip Antenna Design Handbook*. London, U.K.: Artech House, 2001.

[2] S. Gao, L. Ge, D. Zhang, and W. Qin, "Low-profile dual-band stacked microstrip monopolar patch antenna for WLAN and car-to-car communications," *IEEE Access*, vol. 6, pp. 69575–69581, 2018.

[3] T. Wu, H. Su, L. Gan, H. Chen, J. Huang, and H. Zhang, "A compact and broadband microstrip stacked patch antenna with circular polarization for 2.45-GHz mobile RFID reader," *IEEE Antennas Wireless Propag. Lett.*, vol. 12, pp. 623–626, 2013.

[4] A. Katyal and A. Basu, "Compact and broadband stacked microstrip patch antenna for target scanning applications," *IEEE Antennas Wireless Propag. Lett.*, vol. 16, pp. 381–384, 2017.

[5] Y. Li and K.-M. Luk, "A water dense dielectric patch antenna," *IEEE Access*, vol. 3, pp. 274–280, 2015.

[6] L. Ge and K. M. Luk, "Beamwidth reconfigurable magneto-electric dipole antenna based on tunable strip grating reflector," *IEEE Access*, vol. 4, pp. 7039–7045, 2016.

[7] Y. Zhao, Y. Hao, and C. G. Parini, "Radiation properties of PIFA on electromagnetic band gap structures," *Microw. Opt. Technol. Lett.*, vol. 44, no. 1, pp. 21–24, 2005.

[8] I. Ang and B. L. Ooi, "Broadband semi-circle-fed microstrip patch antenna," *Microw., Antennas Propag.*, vol. 1, no. 3, pp. 770–775, 2007.

[9] G. Rafi and L. Shafai, "Broadband microstrip patch antenna with V-slot," *IEE Proc. Microw., Antennas Propag.*, vol. 151, no. 5, pp. 435–440, 2004.

[10] J. Liu, Q. Xue, H. Wong, H. W. Lai, and Y. Long, "Design and analysis of a low-profile and broadband microstrip monopolar patch antenna," *IEEE Trans. Antennas Propag.*, vol. 61, no. 1, pp. 11–18, Jan. 2013.

[11] J. Liu, S. Zheng, Y. Li, and Y. Long, "Broadband monopolar microstrip patch antenna with shorting vias and coupled ring," *IEEE Antennas Wireless Propag. Lett.*, vol. 13, pp. 39–42, 2014.

[12] N. W. Liu, L. Zhu, G. Fu, and Y. Liu, "A low profile shorted-patch antenna with enhanced bandwidth and reduced H-plane cross-polarization," *IEEE Trans. Antennas Propag.*, vol. 66, no. 10, pp. 5602–5607, Oct. 2018.

[13] Y. Cao *et al.*, "Broadband and high-gain microstrip patch antenna loaded with parasitic mushroom-type structure," *IEEE Antennas Wireless Propag. Lett.*, vol. 18, no. 7, pp. 1405–1409, Jul. 2019.

[14] M. R. Ahsan, M. Habib Ullah, F. Mansor, N. Misran, and T. Islam, "Analysis of a compact wideband slotted antenna for *Ku* Band applications," *Int. J. Antennas Propag.*, vol. 2014, 2014, Art. no. 423495.

[15] M. A. Meriche, H. Attia, A. Messai, S. I. M. Sheikh, and T. A. Denidni, "Directive wideband cavity antenna with single layer meta-superstrate," *IEEE Antennas Wireless Propag. Lett.*, vol. 18, no. 9, pp. 1771–1774, Sep. 2019.

[16] S. Lakrit *et al.*, "A new small high-gain wideband rectangular patch antenna for X and Ku bands applications," *J. Taibah Univ. Sci.*, vol. 12, no. 2, pp. 202–207, 2018.

[17] B. Mishra, V. Singh, R. K. Singh, N. Singh, and R. Singh, "A compact UWB patch antenna with defected ground structure for Ku/K band applications," *Microw. Opt. Technol. Lett.*, vol. 60, no. 1, pp. 1–6, 2017.

[18] A. Ghosh, D. Ghosh, S. Chattopadhyay, and L. Lolit Kumar Singh, "Rectangular microstrip antenna on slot-type defected ground for reduced cross-polarized radiation," *IEEE Antennas Wireless Propag. Lett.*, vol. 14, pp. 321–324, 2015.

[19] S. Chakraborty and S. Chattopadhyay, "Substrate fields modulation with defected ground structure: A key to realize high gain, wideband microstrip antenna with improved polarization purity in principal and diagonal planes," *Int. J. RF Microw. Comput. Aided Eng.*, vol. 26, no. 2, pp. 174–181, 2016.

[20] A. Ghosh, S. Chattopadhyay, S. Chakraborty, and B. Basu, "Cross type defected ground structure integrated microstrip antenna: A novel perspective for broad banding and augmenting polarization purity," *J. Electromagn. Waves Appl.*, vol. 31, no. 5, pp. 461–476, 2017.

[21] A. Ghosh, S. Chakraborty, S. Chattopadhyay, and A. Nandi, "Rectangular microstrip antenna with dumbbell shaped defected ground structure for improved cross polarised radiation in wide elevation angle and its theoretical analysis," *Microw., Antennas Propag.*, vol. 10, no. 1, pp. 68–78, 2016.

[22] N. Ripin, S. N. C. Yusoff, A. A. Sulaiman, N. E. A. Rashid, and M. F. Hussin, "Enhancement of bandwidth through I-shaped defected ground structure," in *Proc. IEEE Int. RF Microw. Conf.*, 2013, pp. 477–481.

[23] S. M. D. Abbas *et al.*, "Aspect ratio: A major controlling factor of radiation characteristics of microstrip antenna," *J. Electromagn. Anal. Appl.*, vol. 3, no. 11, pp. 452–457, 2011.

[24] *HFSS-High Frequency Structure Simulator v.14*, Ansoft Corporation, 2014.

[25] S. Chattopadhyay, M. Biswas, J. Y. Siddiqui, and D. Guha, "Input impedance of probe-fed rectangular microstrip antennas with variable air-gap and varying aspect ratio," *Microw., Antennas Propag.*, vol. 3, no. 8, pp. 1151–1156, 2009.

[26] A. Jaiswal, M. P. Abegaonkar, and S. K. Koul, "Highly efficient wideband microstrip patch antenna with recessed ground at 60 GHz," *IEEE Trans. Antennas Propag.*, vol. 67, no. 4, pp. 2280–2288, Apr. 2019.

[27] C.-L. Mak, H. Wong, and K.-M. Luk, "High-gain and wide-band single-layer patch antenna for wireless communications," *IEEE Trans. Veh. Technol.*, vol. 54, no. 1, pp. 33–40, Jan. 2005.

[28] S. Radavaram and M. Pour, "Wideband radiation reconfigurable microstrip patch antenna loaded with two inverted U-Slots," *IEEE Trans. Antennas Propag.*, vol. 67, no. 3, pp. 1501–1508, Mar. 2019.

[29] R. Gomez-Villanueva, R. Linares-y-Miranda, J. A. Tirado-Mendez, and H. Jardon-Aguilar, "Ultra wideband planar inverted-F antenna (PIFA) for mobile phone frequencies and ultra wideband applications," *Prog. Electromagn. Res. C*, vol. 43, pp. 109–120, 2013.

[30] K. Malakar, J. Nandi, S. Mitra, P. K. Gorai, S. Chattopadhyay, and S. Banerjee, "Rectangular microstrip antenna with air cavity for high gain and improved front to back ratio," *J. Electromagn. Anal. Appl.*, vol. 3, no. 9, pp. 368–372, 2011.

[31] G. Fischer, F. Pivit, and W. Wiebeck, "Link budget comparison of different mobile communication systems based on EIRP and EISL," *Adv. Radio Sci.*, vol. 2, pp. 127–133, 2004.